

Magnetic Collapse in Transition Metal Oxides at High Pressure: Implications for the Earth

Ronald E. Cohen,* I. I. Mazin, Donald G. Isaak

Magnetic collapse in transition metal ions is predicted from first-principles computations at pressures reached in the Earth's lower mantle and core. Magnetic collapse would lead to marked changes in geophysically important properties, such as elasticity and conductivity, and also to different geochemical behavior, such as element partitioning, than estimated by extrapolating low-pressure data, and thus change the understanding of Earth's structure and evolution. Magnetic collapse results from band widening rather than from changes in crystal field splitting under pressure. Seismic anomalies in the outer core and the lowermost mantle may be due to magnetic collapse of ferrous iron, dissolved in iron liquid in the outer core, and in solution in magnesiowüstite in the lowermost mantle.

The behavior of major (such as Fe^{2+}) and minor transition metal ions at high pressures plays an important role in understanding Earth's composition and differentiation (1, 2). Using the local density approximation (LDA), the "standard model" of first-principles solid-state electronic structure methods, Isaak *et al.* (3) predicted that FeO would undergo magnetic collapse (that is, a high-spin low-spin transition) possibly within pressures attained within the Earth. We obtained more accurate predictions of magnetic collapse in transition metal oxide compounds, using an improved (4, 5) theory, the generalized gradient approximation (GGA), and extended our previous studies of magnetic collapse to Fe^{2+} in FeO with the NiAs structure (called B8) and in FeSiO_3 perovskite, and to other transition metal ions such as Mn^{2+} , Co^{2+} , and Ni^{2+} . We found that magnetic collapse occurs in all these magnetic transition metal ions, in some cases at experimentally accessible pressures. We also present a physical interpretation of the predicted behavior that allows extrapolation to more complex phases and solid solutions that are important in geochemistry.

A material can undergo a magnetic transition (6) because of band widening or because of changes in the crystal field (7). In the Stoner model (8), a magnetic state is stable if $IN(0) > 1$, where the Stoner integral I is determined by the self-consistent spin splitting of atomic d -states induced by an applied magnetization M , and $N(0)$ is the density of states at the Fermi level. This

criterion is derived from minimization of the sum of the magnetic energy, $-M^2/2$, and the change in the band energy, $M^2/2N(0)$, for magnetization M . Under com-

pression, I changes little but $N(0)$ decreases as the bandwidth increases. At a critical pressure, the Stoner criterion is not satisfied, and the system becomes nonmagnetic. Magnetic collapse could also occur if the crystal field splitting becomes larger than the exchange splitting, in which case the occupancy of states changes and the magnetic moments collapse. In the more refined extended Stoner theory (9), the average density of states is introduced, $\bar{N}(M) = M/\Delta\epsilon$, where $\Delta\epsilon$ is the spin splitting. The criterion for a magnetic state to exist is $I\bar{N}(M) = 1$. Note that $\bar{N}(0) = N(0) = \partial M/\partial\Delta\epsilon$. The extended Stoner calculations bridge the gap between the localized approach (crystal field-induced) and the conventional Stoner theory.

We investigated the magnetic properties at very high pressure of FeO, MnO, CoO, NiO, and FeSiO_3 perovskite using first-principles linear muffin tin orbital (LMTO) and linearized augmented plane wave

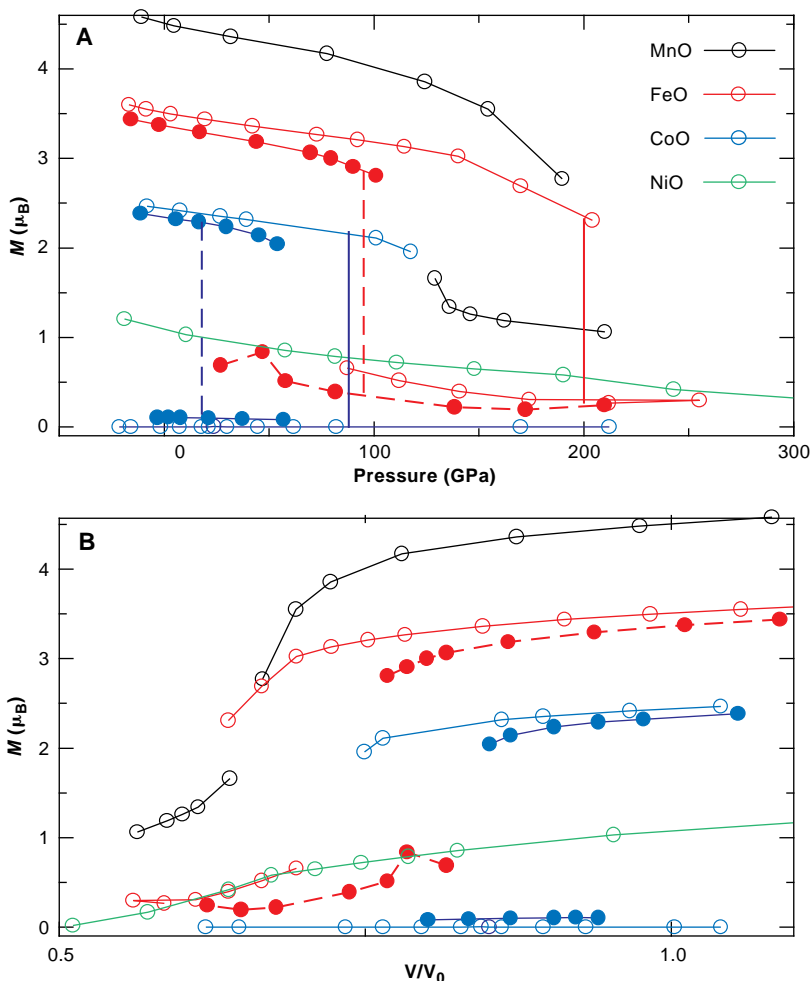


Fig. 1. Magnetic moments M [in Bohr magnetons (μ_B)] for antiferromagnetic transition metal oxides in the B1 structure as a function of (A) pressure and (B) compression computed self-consistently with the LMTO-ASA method. Compression was calculated with respect to the theoretical zero pressure volumes. GGA results (open circles) are shown for MnO, FeO, CoO, and NiO; LDA results (solid circles) are shown for FeO and CoO for comparison. Vertical lines denote transition pressures.

R. E. Cohen and I. I. Mazin, Geophysical Laboratory and Center for High-Pressure Research, Carnegie Institution of Washington, 5251 Broad Branch Road, NW, Washington, DC 20015, USA.

D. G. Isaak, Institute of Geophysics and Planetary Physics, University of California at Los Angeles, Los Angeles, CA 90095-1567, and Department of Mathematics and Physics, Azusa Pacific University, Azusa, CA 91702, USA.

*To whom correspondence should be addressed.

(LAPW) electronic structure methods within the GGA (10, 11). Our equations of state (Table 1) show that GGA models the compression of transition metal oxides accurately. We computed the antiferromagnetic moments for cubic rocksalt (B1)-structured FeO, MnO, CoO, and NiO (Fig. 1 and Table 2) and found that all four compounds exhibit magnetic collapse. The LDA transition pressures were lower than the GGA transition pressures, because LDA underestimates magnetic stabilization energies (12). For FeO, magnetic collapse occurred at relatively high pressures (13), whereas for CoO, the transition pressure was relatively low. We found first-order transitions with significant (5 to 7%) fractional volume changes, $\Delta V/V$, except for NiO, where the magnetic moment decreased gradually. Thus, in FeO, CoO, and MnO, the transitions could be detected experimentally with standard x-ray diffraction techniques and by looking for a volume discontinuity in the equation of state. Because CoO, unlike FeO, is stoichiometric and has the lowest transition, it should be the most amenable to experimental study.

The methods we use are the most appropriate tractable methods to study properties of transition metal oxides in the high-pressure regime where bandwidths are large (14). At low pressures, there are inadequacies in both GGA and LDA; for example,

they predict metallic behavior for FeO and CoO, which are insulators. This is due to the neglect of strong correlations of localized electrons, characterized by a parameter called the Hubbard U , that inhibits multiple occupation of d orbitals on the same metal ion; U is the energy increase when an additional electron is added to a d orbital. The parameter that governs the tendency toward localization is U/W , where W is the bandwidth. Materials that are Mott or charge transfer insulators at low pressures will become metallic with increasing pressure because W increases with pressure and U decreases because of increased screening. Thus, at high pressures, band theory should be quite reliable. Recent many-body Monte Carlo simulations predicted metallic behavior for $U/W < \sqrt{N}$ (15), where N is the orbital degeneracy (5 in our case), so that at the pressures of interest here, band theory should be applicable (Table 3) (16). Another important study showing the accuracy of our approach used the same methods and predicted magnetic collapse and metallization of NiI_2 at 25 GPa (17), compared with the experimental value of 19 GPa (18).

We performed an extended Stoner analysis (Fig. 2) and found that it accurately predicted the behavior we found in our self-consistent computations. This demonstrates that magnetic collapse occurs because of band broadening with pressure,

with very little change in crystal field. The crystal field and structural details govern the shape of the effective density of states and thus govern the character of the magnetic collapse (that is, whether it is continuous or discontinuous, as well as the magnitudes of the high- and low-spin moments at a given pressure). The shape of the effective density of states does not change much with pressure; it is primarily the uniform decrease in effective densities of states that gives rise to magnetic collapse. The existence of a low-spin state is due to the crystal field splitting, which manifests itself by a dip in the density of states between the centers of the t_{2g} and e_g bands. However, the transition is not due to changes in the

Table 1. Theoretical and experimental parameters from GGA computations of antiferromagnetic transition metal monoxides at zero pressure. Experimental parameters are listed in parentheses. Volumes are for the primitive antiferromagnetic cell (four atoms). Experimental data are from (28) for MnO, (3) for FeO, (29) for CoO, and (30) for NiO. V_0 , zero pressure volume; K , bulk modulus; and K' , dK/dP .

Monoxide	V_0 (bohr ³)	K (GPa)	K'
MnO	303 (296)	196 (170)	3.9 (4.8)
FeO	280 (275)	178 (142-180)	4.2 (4.9)
CoO	265 (261)	177 (181)	5.4
NiO	253 (246)	194 (166-208)	4.5

Fig. 2. (A) Extended Stoner diagram (effective density of states versus local magnetic moment in states per rydberg) for CoO for cell volumes 266 ($P = 0$), 228 ($P = 40$ GPa), and 210 bohr³ ($P = 90$ GPa) (1 bohr³ = 0.14818 Å³). The horizontal line denotes the inverse Stoner integral I for a Co²⁺ ion. The heavy solid line (top) shows the limit of infinitely narrow bands (localized limit for an isolated ion). The crossings with I/I give potential magnetic states with moment M ; only crossings with negative slope are stable or metastable states. Thus, at $V = 266$ bohr³, there is only high-spin Co²⁺, with $M = 2.8 \mu_B$; at 228 bohr³ there is a high-spin state of $M = 2 \mu_B$ and a low-spin state with $M = 0.3 \mu_B$ (total energy calculations show the high-spin state to have lower free energy here), and at 210 bohr³ there are no magnetic solutions. (B) Similar diagram for FeSiO₃ and SiFeO₃ at $V = 216$ bohr³ ($P = 200$ to 300 GPa). Note the different shape and magnitude of $\tilde{N}(M)$, from which one can predict that the former compound will undergo magnetic collapse and the latter will undergo gradual demagnetization. (C) Similar diagram for FeO in the B8 structure at $V = 158$ bohr³ ($P = 700$ GPa).

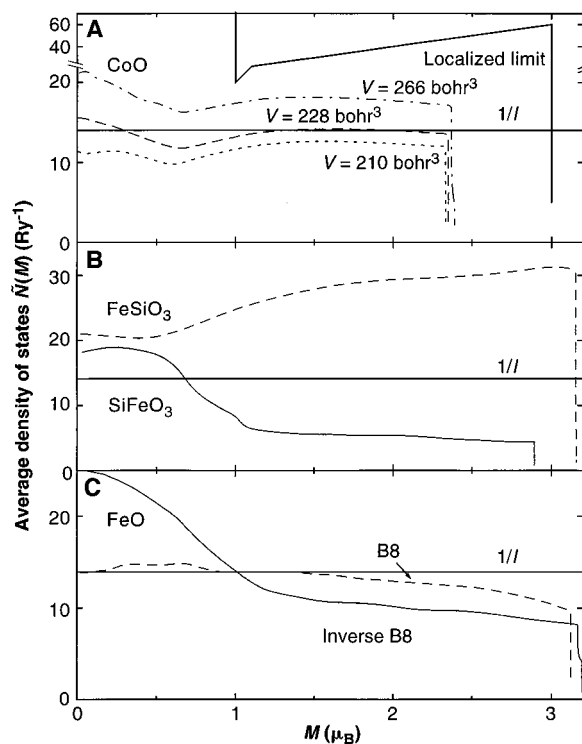


Table 2. Parameters (from GGA computations) for the high-low spin transition. V_{low} and V_{high} are the volumes (in bohr³) of the low- and high-spin phases, respectively; M_{low} and M_{high} are the corresponding respective magnetizations (in μ_B). P_{tr} is the transition pressure in gigapascals. Parameters derived from LDA computations are listed in parentheses.

Parameter	MnO	FeO	CoO	NiO
V_{low}	182	166 (183)	193 (213)	166
V_{high}	209	180 (197)	206 (227)	167
M_{low}	1.3	0.3 (0.3)	0.0 (0.1)	0.0
M_{high}	3.4	2.3 (2.8)	2.2 (2.3)	0.6
P_{tr}	149	200 (95)	88 (18)	230

Table 3. Hubbard parameter U (31) and effective bandwidths W (32) at 0 GPa and at magnetic collapse pressures in electron volts. The critical value of U/W is 2.24, so band theory should be appropriate at the high pressures where magnetic collapse occurs.

Parameter	MnO	FeO	CoO	NiO
U ($P = 0$)	7.8	5.1	5.3	6.7
W ($P = 0$)	1.0	0.9	1.0	1.4
W (P_{tr})	3.5	3.4	3.0	3.5
U/W ($P = 0$)	7.8	5.7	5.3	4.8
U/W (P_{tr})	2.2	1.5	1.8	1.4

crystal field splitting with pressure, which are quite small.

A crucial question is the importance of the ionic environment. Magnetic collapse in strained B1 occurs at similar pressures as in cubic B1 (3). There are two possible crystallographic modifications of the B8 structure, depending on whether Fe is in the Ni (normal B8) or the As (inverse B8) sites. In normal B8, the Fe atoms form chains along *c* (the hexagonal axis), and magnetic collapse is continuous. In contrast, there is a more sudden transition in inverse B8 but only at extreme pressures (>500 GPa). The continuous transition in normal B8 occurs because the short Fe-Fe distances along *c* lead to a highly dispersive d_{z^2} band, which makes the t_{2g} sub-band very wide. The extended Stoner picture correctly predicts the behavior we observe in our self-consistent computations. Given that the local environment is crucial and that collapse is not related to cooperative effects such as magnetic ordering, defects such as the observed nonstoichiometry in FeO at low pressures will not directly influence the predicted transition.

We also studied FeSiO₃ perovskite, which is not stable relative to FeO + SiO₂ stishovite. Understanding Fe behavior in silicate perovskite is extremely important, because (Mg,Fe)SiO₃ perovskite containing up to 15% Fe is considered to be the most common mineral in the Earth. We considered Fe in either the A or the B sites of the structure (19, 20); in both cases, the Fe atoms are at the same distance from each other, too far apart for significant Fe-Fe hopping. Iron is high-spin in the A site and low-spin in the B site at geophysically relevant pressures (<135 GPa). In the A site, collapse did not occur until 1 TPa, whereas in the B site, the magnetic moment decreased smoothly from high spin at low pressures to low spin at high pressures. We found the crystal field $t_{2g}-e_g$ splitting to be nearly the same in the two structures at all pressures. The B site is much smaller than the A site, so that the bandwidths are much larger when Fe is in the B site, thus leading to different magnetic behavior and again showing that magnetic collapse is governed by the bandwidth, not the crystal field.

Transition pressures will depend on the local structure and "compression" of the ion. For example, transition metal sulfides and iodides tend to have lower pressure transitions because the greater overlap with the larger anions leads to larger bandwidths. Thus, in NiI₂ magnetic collapse occurs at 19 GPa (18), whereas we predict collapse at 230 GPa in NiO. This phenomenon is evident in the system FeS₂-MnS₂ (21). Ferrous iron in FeS₂ is low spin, whereas dilute Fe²⁺ in MnS₂, which has a larger molar

volume than FeS₂, is high spin. In the lightly doped material, the Fe²⁺ ions undergo magnetic collapse to low spin under moderate compression (12 GPa). Thus, compression of Fe²⁺ by applied pressure or by substitution in a smaller structural site will induce magnetic collapse. This is completely consistent with our results on Fe-SiO₃. Ferrous iron in magnesiowüstite will undergo magnetic collapse at lower pressures than will pure FeO, because the Mg²⁺ ion is smaller than the Fe²⁺ ion.

The potential geophysical and geochemical implications of these results are extensive and highlight the need for experimental studies of the behavior of transition metal oxides and silicates at pressures >100 GPa. We outline some of the most important implications. Of the transition metals, only Fe²⁺ is sufficiently abundant to affect the structure and seismic properties of the Earth. We find a transition pressure of 200 GPa for FeO, which is appropriate to the outer core (22). This is intriguing, because magnetic collapse in Fe²⁺ ions could occur in an iron-rich liquid and would cause density and elastic anomalies. Some seismic studies do indeed provide evidence that the Earth's outer core is stratified (23). Ferrous iron in magnesiowüstite will collapse at lower pressures than ferrous iron dissolved in Fe liquid, as a result of the environmental effect discussed above. Thus, magnetic collapse may also be partly responsible for anomalies in *D''*, that is, the complex region in the lower mantle immediately above the iron core (24, 25), where Fe is present mostly as magnesiowüstite, as well as in the core.

A long-standing problem has been the excess of siderophile elements in Earth's mantle relative to the lithophile elements (26). Changes in the nature of bonding brought on by magnetic collapse at high pressure means that extrapolation of low-pressure results will have little applicability to siderophiles at lower mantle pressures. Our results apply most directly to Ni and Co, which require nearly equal partition coefficients to explain their similar depletions in the mantle, whereas low-pressure experiments show Ni to be more siderophile than Co (27). Magnetic collapse in Co²⁺ would make it more siderophile, and would thus help to explain the relative depletions of Ni and Co. Our results show the importance of further partitioning experiments at ultrahigh pressures appropriate to Earth's lower mantle.

The high-spin low-spin magnetic transitions in transition metal oxide compounds obtained in our computations range from 90 GPa for CoO to 1 TPa in FeSiO₃. These theoretical predictions must be tested in the laboratory, but on the basis of previous stud-

ies, we estimate a maximum uncertainty of 30 GPa in our GGA transition pressures. Our calculations demonstrate that the band broadening due to shorter nearest neighbor distances, not an increase of the crystal field splitting, causes collapse of the high-spin magnetic state under pressure. The resulting changes in bonding character from ionic to metallic would also affect mineral stability. Charge would move out of the bonding directions and shapes of the transition metal and oxygen ions would change, affecting phase diagrams and elasticity. Transition metal ions will behave essentially as "different elements" at high pressures, and chemical intuition derived from experience at low pressures will not be applicable. Even the concept of chemical valence is not appropriate at ultrahigh pressures.

REFERENCES AND NOTES

1. V. R. Murthy, *Science* **253**, 303 (1991).
2. D. Walker, L. Norby, J. H. Jones, *ibid.* **262**, 1858 (1993).
3. D. G. Isaak, R. E. Cohen, M. J. Mehl, D. J. Singh, *Phys. Rev. B* **47**, 7720 (1993).
4. D. M. Sherman and H. J. F. Jansen, *Geophys. Res. Lett.* **22**, 1001 (1995).
5. P. Dufek, P. Blaha, V. Sliwko, K. Schwarz, *Phys. Rev. B* **49**, 10170 (1994).
6. We are not considering magnetic transitions involving ordering and disordering of spins as in a Néel transition, but rather electronic transitions that change the magnitudes of spin moments.
7. S. Ohnishi, *Phys. Earth Planet. Inter.* **17**, 130 (1978).
8. E. C. Stoner, *Proc. R. Soc. London Ser. A* **169**, 339 (1939).
9. G. L. Krasko, *Phys. Rev. B* **36**, 8565 (1987); O. K. Andersen *et al.*, *Physica B+C*, **86-88 B+C**, 249 (1977).
10. J. P. Perdew and Y. Wang, *Phys. Rev. B* **45**, 13244 (1992).
11. We used density functional theory (DFT) methods, which are first principles in that they require no experimental input other than the nuclear charges and positions. LMTO-atomic sphere approximation (ASA) is a fast method that neglects nonspherical contributions to the potential. The LAPW method is among the most accurate electronic structure methods that assume no shape approximations. We compared LMTO-ASA results for CoO and FeO in the LDA approximation with the full-potential LAPW method and found satisfactory agreement. Equations of state are practically the same. The energy differences between high- and low-spin configurations had an error of tens of millirydbergs compared with LAPW, and LMTO transition pressures were about 20 GPa different from LAPW. We found no sensitivity to the number of *k* points (reciprocal lattice points used in Brillouin zone integrals), atomic sphere radii, or basis set sizes.
12. L. Stixrude, R. E. Cohen, D. J. Singh, *Phys. Rev. B* **50**, 6442 (1994).
13. Collapse in B1 is above the structural transition into the B8 structure at high temperatures, although strained B1 can be maintained metastably to high pressures at room temperature [Y. Fei and H.-k. Mao, *Science* **266**, 1678 (1994)].
14. Other available approaches would not be appropriate for this study. Hartree-Fock methods give excellent results for energetics in transition metal oxides at zero pressure but severely overestimate insulating gaps and are inapplicable for metals or for metal-insulator transitions. The B8 structure of FeO is metallic [X. Li and R. Jeanloz, *Geophys. Res. Lett.* **21**, 2183 (1994)]. More exact methods such as GW [F. Aryasetiawan and O. Gunnarsson, *Phys. Rev. Lett.*

- 74, 3221 (1995)] are not tractable for the large number of structures and pressures necessary for this study.
15. O. Gunnarsson, E. Koch, R. M. Martin, *Phys. Rev. B* **54**, R11026 (1996).
 16. Similarly, conventional LDA calculations accurately predict properties of the perovskites, La(Mn,Fe,Co,Ni)O₃ [D. D. Sarma *et al.*, *Phys. Rev. Lett.* **75**, 1126, (1995)], because the transition metal hopping integrals are ~40% larger than in binary oxides and the screened U is ~40% smaller.
 17. P. Dufek, P. Blaha, K. Schwarz, *Phys. Rev. B* **51**, 4122 (1995).
 18. M. P. Pasternak *et al.*, *Phys. Rev. Lett.* **65**, 790 (1990).
 19. W. E. Jackson, E. Knittle, G. E. Brown Jr., R. Jeanloz, *Geophys. Res. Lett.* **14**, 224 (1987).
 20. We found the normal perovskite with Fe in the A site to be 4.6 eV (440 kJ/mol) lower in energy than that with Fe in the B site (LAPW, LDA). We also found wüstite plus stishovite to be lower in energy than FeSiO₃ at all pressures, which is consistent with the small solubility of Fe in silicate perovskite. Orthorhombic MgSiO₃ was lower in energy than stishovite plus periclase at all pressures, which is consistent with the lack of observed breakdown of MgSiO₃ at low temperatures. However, cubic MgSiO₃ was marginally unstable with respect to periclase plus stishovite.
 21. C. B. Barger, M. Avinor, H. G. Drickamer, *Inorg. Chem.* **10**, 1338 (1971); H. G. Drickamer and C. W. Frank, *Electronic Transitions and the High Pressure Chemistry and Physics of Solids* (Halsted, New York, 1973), pp. 126–129.
 22. Temperatures are about 2000 K in the lower mantle and higher in the core. We can estimate the effects of temperature from the Clapeyron equation $dP/dT = \Delta S/\Delta V$, where P is pressure, T is temperature, S is entropy, and V is volume. We use the upper bound for the magnetic entropy $S_{\text{mag}} = R \ln(M + 1)$, where R is the gas constant. For FeO, we estimate a bound of $dP/dT < 0.015$ GPa/K, which is close to the estimate of 0.01 GPa/K of Ohnishi (7). Thus, we expect an increase of about 29 GPa in transition pressure at 2000 K.
 23. T. Lay and C. J. Young, *Geophys. Res. Lett.* **17**, 2001 (1990).
 24. E. Knittle and R. Jeanloz, *Science* **251**, 1438 (1991).
 25. D. E. Loper and T. Lay, *J. Geophys. Res.* **100 B4**, 6397 (1995).
 26. H. E. Newsom and K. W. W. Sims, *Science* **252**, 926 (1991).
 27. A. Holzheid and H. Palme, *Geochim. Cosmochim. Acta* **60**, 1181 (1996).
 28. R. Jeanloz and A. Rudy, *J. Geophys. Res.* **92**, 11433 (1987).
 29. N. Uchida and S. Saito, *J. Acoust. Soc. Am.* **51**, 1602 (1972).
 30. E. Huang, K. Jy, S.-C. Yu, *J. Geophys. Soc. China* **37**, 7 (1994).
 31. V. I. Anisimov, J. Zaanen, O. K. Andersen, *Phys. Rev. B* **44**, 943 (1991).
 32. We estimated the effective W by taking the total d band width and subtracting Δ , the splitting between e_g and t_{2g} , from our computations.
 33. Supported by NSF grant EAR-9418934. Computations were performed on the Cray J90 at the Geophysical Laboratory. D.G.I. was supported in part by the U.S. Office of Naval Research and NSF grant EAR-9405965. We thank O. K. Andersen, Y. Fei, R. Hazen, R. Hemley, H. Krakauer, C. T. Prewwitt, D. J. Singh, and L. Stixrude for helpful discussions.

5 July 1996; accepted 26 November 1996

A General Strategy for Selecting High-Affinity Zinc Finger Proteins for Diverse DNA Target Sites

Harvey A. Greisman and Carl O. Pabo*

A method is described for selecting DNA-binding proteins that recognize desired sequences. The protocol involves gradually extending a new zinc finger protein across the desired 9- or 10-base pair target site, adding and optimizing one finger at a time. This procedure was tested with a TATA box, a p53 binding site, and a nuclear receptor element, and proteins were obtained that bind with nanomolar dissociation constants and discriminate effectively (greater than 20,000-fold) against nonspecific DNA. This strategy may provide important information about protein-DNA recognition as well as powerful tools for biomedical research.

Design of DNA-binding proteins that will recognize desired sites on double-stranded DNA has been a challenging problem. Although a number of DNA-binding motifs have yielded variants with altered specificities, zinc finger proteins related to TFIIIA (1) and Zif268 (2) appear to provide the most versatile framework for design. Modeling, sequence comparisons, and phage display have been used to alter the specificity of an individual zinc finger within a multifinger protein (3–7), and fingers also have been “mixed and matched” to construct new DNA-binding proteins (8, 9). These design and selection studies have assumed that each finger [with its corresponding 3-base pair (bp) subsite] can be treated as an independent unit (Fig. 1B). This assumption has provided a useful starting point for design studies, but crystallographic

studies of zinc finger–DNA complexes (10–13) reveal many examples of contacts that couple neighboring fingers and subsites, and it is evident that context-dependent interactions are important for zinc finger–DNA recognition (3, 7, 8). Existing strategies have not taken these interactions into account in the design of multifinger proteins, and this may explain why there has been no effective, general method for designing high-affinity proteins for desired target sites (14).

We have developed a selection strategy that can accommodate many of these context-dependent interactions between neighboring fingers and subsites. Our strategy involves gradual assembly of a new zinc finger protein at the desired binding site—adding and optimizing one finger at a time as we proceed across the target site. We use the Zif268 structure (10, 13) as our framework and randomize six potential base-contacting positions in each finger (Fig. 1, A and D) (15). Our protocol includes three selection steps (Fig. 2), one for each finger of the new

protein: (i) A finger that recognizes the 3' end of the target site is selected by phage display (Fig. 2A). At this stage, two wild-type Zif fingers are used as temporary anchors to position the library of randomized fingers over the target site, and we use a hybrid DNA site that has Zif subsites fused to the target site. (ii) The selected finger is retained as part of a “growing” protein and, after the distal Zif finger is discarded, phage display is used to select a new finger that recognizes the central region of the target site (Fig. 2B). (iii) Finally, the remaining Zif finger is discarded, and phage display is used to select a third finger that recognizes the 5' region of the target site (Fig. 2C). Optimization of this finger yields the new zinc finger protein.

Our strategy ensures that the new fingers are always selected in a relevant structural context. Because an intact binding site is present at every stage, and because our selections are performed in the context of a growing protein–DNA complex, our method readily optimizes context-dependent interactions between neighboring fingers and subsites and naturally selects for fingers that will function well together (16). To ensure that the selected proteins will bind tightly and specifically to the desired target sites, we performed all selections in the presence of calf thymus competitor DNA (3 mg/ml) (17). This serves to counterselect against any proteins that bind promiscuously or prefer alternative sites, and our protocol thus directly selects for affinity as well as specificity of binding (18).

We tested our protocol by performing selections with a TATA box, a p53 binding site, and a nuclear receptor element (NRE) (Fig. 1C). These important regulatory sites were chosen because they normally are recognized by other families of DNA-binding proteins and because these sites are quite

Howard Hughes Medical Institute and Department of Biology, Massachusetts Institute of Technology, Cambridge, MA 02139, USA.

*To whom correspondence should be addressed.